Novel epoxy powder for manufacturing thick-section composite parts under vacuum-bag-only conditions. Part II: Experimental validation and process investigations

Citation for published version:
Maguire, J, Nayak, K & O Brádaigh, C 2020, 'Novel epoxy powder for manufacturing thick-section composite parts under vacuum-bag-only conditions. Part II: Experimental validation and process investigations', *Composites Part A: Applied Science and Manufacturing*, vol. 136, 105970. https://doi.org/10.1016/j.compositesa.2020.105970

Digital Object Identifier (DOI):
10.1016/j.compositesa.2020.105970

Link:
Link to publication record in Edinburgh Research Explorer

Document Version:
Peer reviewed version

Published In:
Composites Part A: Applied Science and Manufacturing

Novel epoxy powder for manufacturing thick-section composite parts under vacuum-bag-only conditions. Part II: Experimental validation and process investigations

James. M. Maguire [a,*], Kapileswar Nayak [b], Conchúr M. Ó Brádaigh [a]

[a] *School of Engineering, Institute for Materials and Processes, The University of Edinburgh, Edinburgh, EH9 3FB, UK*

[b] *Suzlon Energy Limited (NL Branch), Jan Tinbergenstraat 290, 7559 ST Hengelo (Overijssel), The Netherlands*

* *Corresponding author. Email address: j.maguire@ed.ac.uk*

Abstract

Validations of a one-dimensional process model are carried out by manufacturing thick-section glass-fibre reinforced composite laminates with a low-exotherm epoxy powder. An experimental apparatus is developed which heats the laminates from one side while insulating the remaining sides (i.e. approximating one-dimensional heat transfer conditions). Temperatures within the laminate are measured using thermocouples and a linear variable differential transformer is used to measure the thickness change of the laminate, with respect to time, due to powder sintering and fabric impregnation. The experimental results are analysed and used to validate process models for the epoxy powder system. Process simulations are performed to analyse the influence of material format, laminate thickness change, and heating methods (i.e. one-sided heating vs two-sided heating, and heated tooling vs oven heating). It is shown that epoxy powder eliminates the risk of 'thermal runaway', but thermal and cure gradients persist for a conventional processing cycle. Methods to inhibit the evolution of these gradients are explored using process simulations. These methods include modifying the temperature cycle and using multiple epoxy powders with varied latent curing properties.

Keywords: A. Epoxy powder, C. Process simulation, D. Process monitoring, E. Out of autoclave processing.

1. Introduction

The processing of thick-section composite structures with thermoset resins is a challenge due to the exothermic heat produced by the curing reaction and the low thermal conductivity of the materials involved. The enthalpy of reaction for conventional epoxy systems is typically 400-500 J/g [1–3], while the thermal conductivities of both epoxy resin and dry reinforcing fabric (in the through-thickness direction) range in the order of 0.1 W/m K [4–8]. As a result, heat is slow to transfer out of thick laminates; this increases the temperature of the resin within, promotes further curing, and releases more heat until the reaction ceases. This auto-accelerative curing phenomena is also known as ‘thermal spiking’, ‘thermal overshoot’ or ‘thermal runaway’ [9]. It can cause thermal degradation of the polymer matrix, fibre-matrix interface and bagging materials, and can also cause component warpage [10,11]. In any case, the manufacturer would incur significant financial repercussions from having to scrap large expensive components, so careful development is required.

To reduce the risk of ‘thermal runaway’, low-exotherm systems can be used when processing thick-section composite parts. One such material system that has received significant attention for composite applications is epoxy powder [12–15]. It has been shown that epoxy powders can be formulated to function very effectively as the primary polymer matrix within composite structures. Typically, the epoxy powder is dispersed on a dry fabric and processed as a vacuum-bag-only (VBO) prepreg, a.k.a. an out-of-autoclave (OoA) prepreg, due to its relatively low viscosity (minimum viscosity of approximately 1 Pa s [12]). While the system has shown great potential, the aforementioned research has been focused, predominantly, on small samples of epoxy powder and thin laminates which have been carefully processed with a specific temperature cycle. As such, to determine whether its advantages can be exploited at an industrial scale, it is important to understand how the material behaves in thicker sections which undergo greater temperature variation.

In Part I of this work [16], one-dimensional (1D) process models were developed for powder-based systems, with a specific focus on epoxy powders. These models were used to numerically simulate the processing of a thick-section composite laminate for a standard temperature cycle. This paper will focus on experimental validation of the 1D process models described in Part I [16] as well as further numerical simulations aimed at reducing potential temperature and cure gradients in processing of thick-section laminates.

The literature on VBO prepreg processing has focussed predominantly on thin laminates where a uniform temperature distribution could be assumed in the through-thickness direction. Consequently, heat transfer analysis of the thin laminates was not necessary and resin flow could be measured either in-situ or ex-situ for a given test temperature. Centea and Hubert [17,18] were able to freeze thin laminates (consisting of 4 plies) in a partially impregnated state by rapidly cooling them at various stages during a standard temperature cycle. They then performed X-ray microtomography (micro-CT or μ-CT) to measure the resin flow front position within a tow for the given time and temperature profile. While this method was very intuitive for studying the progression of resin flow within a tow, the frequency of data collection was low, and the samples had to be small (< 15 mm × 15 mm) to capture flow front position. In contrast, Cender *et al.* [19] experimentally validated their resin flow model using an in-situ method. Under isothermal conditions, a charge-coupled device (CCD) camera was used to track flow front progression through a transparent tool. This method provided much greater data resolution for validating the resin flow model, however, it was limited to single ply tests as the camera could only track resin flow on the dry side of the ply. A later study by Centea and Hubert [20] examined the consolidation of VBO prepregs under deficient pressure conditions. They developed an experimental apparatus which could measure the thickness change of a thin laminate using a non-contact sensor. Although, this method did not give a direct visualisation of the flow progression, they were able to analyse the final state of the cured laminates using optical microscopy. They found that the laminate thickness reduced during air evacuation and resin flow, and the rate of thickness change was affected by pressure conditions such that entrapped gases would resist resin flow, resulting in macroscopic and microscopic voids. Helmus *et al.* [21] used these experiments to validate their models for air evacuation and resin flow; achieving good agreement for thickness change. They showed that the laminate underwent a total thickness reduction of approximately 30% during air evacuation and fibre-bed impregnation.

Laminate thickness change has also been used to validate resin flow and consolidation models for thick-section laminates. Gutowski *et al.* [22] developed a specialised compression die which could measure the resin pressure in a laminate and the thickness change as a controlled load was applied using an Instron Test Machine. Shin and Hahn [23] manufactured thick prepreg laminates (30 - 50 mm thick) in a heated press and validated their coupled resin flow and heat transfer model by monitoring the distance between the heated platens and measuring the temperature through the thickness of the centre of the laminate using thermocouples. For models with a 1D, through-thickness heat transfer assumption, the laminate edges were insulated (e.g. by fibreglass or silicone rubber) [5,7,9,23–25].

For this project, simulations were initially compared to thermocouple data for a 96-ply glass-fibre (GF)/Epoxy-powder laminate which was processed in an oven [26] – the data was provided by an industry partner (ÉireComposites Teo.). While the results were promising, the thickness was not measured in-situ and therefore it was not possible to validate the consolidation models from Part I [16]. Moreover, the conditions within the oven were unknown w.r.t. the heat transfer coefficient (HTC). As a result, the thermal boundary conditions (BCs) of the simulation had to be fitted to the experimental data. For improved validation, an experimental apparatus was developed which could measure the thickness change of the laminate and approximate 1D heat transfer conditions [27]. The results showed that the processing models for resin flow and heat transfer closely matched with the experimental data, but that thickness change due to sintering could not be described by DSC data alone. Consequently, additional experiments were performed to characterise and model the sintering process, which are described in Part I [16].

For this paper, the design of the experimental apparatus is presented along with details of the hardware and signal analysis used to measure temperature and thickness change. Experimental data for 3 thick-section laminates is compared with simulated results to validate the process models. Additional simulations are presented which investigate the format of the vacuum-bag-only (VBO) prepreg, the importance of thickness change, heating methods, and methods for improving the manufacturing process.

2. Materials and Methodology

2.1 Material Format

Two material formats were investigated:

- A 1200 gsm, stitched uni-directional (UD) glass fabric (086 sizing) supplied by Johns Manville [28], with loose epoxy powder (GRN-918) manually dispersed between each ply [29].
- An 1800 gsm, stitched triaxial glass fabric that had been partially impregnated from one side with GRN-918 using an automated process. This VBO prepreg (a.k.a. semi-preg) was supplied by ÉireComposites Teo.

2.2 Experimental Apparatus Design

As illustrated in Figure 1, the design concept was to manufacture thick-section laminates on a heated tool, and use 200 mm thick glass wool insulation slabs to control the top and side boundary conditions. The temperatures would be measured using thermocouples and the thickness change would be measured using one or more linear variable differential transformers (LVDTs). LVDTs were chosen because they offer high resolution and a measurement range of >100 mm, making them well suited to the measurement of large thickness changes.

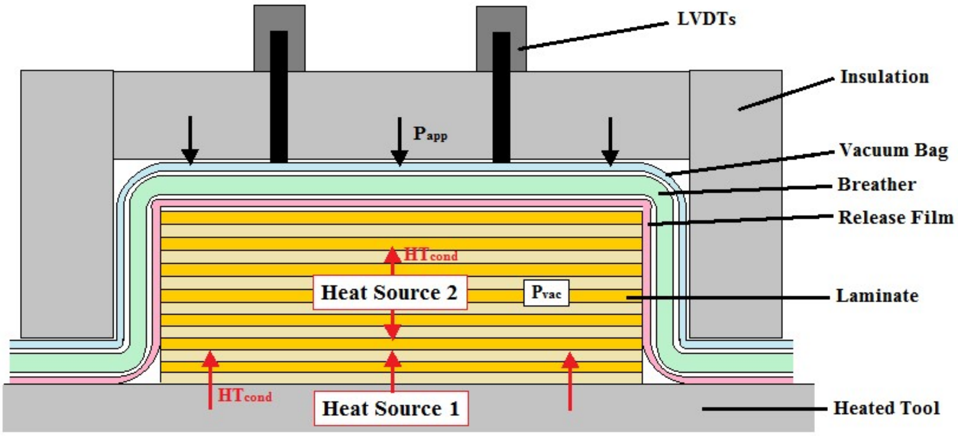

Figure 1. Conceptual design for the experimental validation apparatus. Note: heat source 1 is the heated tool, while heat source 2 is heat generated by the exothermic curing reaction within the laminate.

Figure 2. Photo of the heated tool and tool frame.

An existing heated tool, shown in Figure 2, was chosen as the primary heat source for the apparatus design. The heated tool consisted of a 610 mm × 610 mm × 10 mm flat aluminium plate with a 600 mm × 600 mm silicone rubber heating mat adhesively glued to the underside of the plate. The plate was supported at its edges by vermiculite slabs which have a low thermal conductivity (0.1 – 0.15 W/m K). An additional 100 mm thick glass wool insulation slab was placed underneath the tool to insulate it further. This insulated the plate from the main tool frame and improved the temperature uniformity across the plate.

2.3 Instrumentation and Signal Analysis

A Monitran economy series, spring-loaded, AC LVDT was used for measuring the thickness change. The LVDT had a stroke of ± 50 mm and a 4-wire connection. A FeelTech arbitrary function signal generator was used to generate a 3 kHz AC signal with an amplitude of 7.07V (5V RMS). This input signal, along with the output signal of the secondary windings, was fed into a National Instruments (NI) USB 6009 (analog) module. Analysis of the LVDT signal was performed in LabVIEW. The LabVIEW program recorded the voltage amplitude and phase of the secondary winding, then used a linear relationship (voltage divided by a slope of 0.01154) to calculate the displacement of the core. As a 3 kHz signal was used, the program cycle only ran every 1 min to reduce the amount of data that was stored.

The LabVIEW program recorded temperature data from K-type thermocouples via two NI 9211 modules (four thermocouples each). In addition to this, a Pico USB TC-08 thermocouple data logger was used to record temperatures from eight additional K-type thermocouples.

2.4 Laminate Manufacturing

The first test laminate, henceforth referred to as Test Laminate 1, consisted of 60 plies of UD GF with GRN-918 powder manually dispersed between each GF ply. The weight of powder for each layer was measured so that a fibre volume fraction (FVF) of 0.5 was targeted. The lay-up of this laminate is shown in Figure 3(a), along with the lay-up of the second laminate, Test Laminate 2 (Figure 3(b)). Test Laminate 2 consisted of 44 plies of triaxial semi-preg. The automated prepregging process deposited sufficient resin for a target FVF of 0.5 also. An additional laminate, Test Laminate 3, was manufactured as a repeat of Test Laminate 1, but consisted of 48 plies and had a target FVF of 0.45. This lower FVF was targeted due to the presence of voids in Test Laminate 1. This is discussed further in the results and discussion section.

Figure 3. Lay-up of the thick-section laminates on the heated tool: (a) GRN 918 epoxy powder was weighed and then manually dispersed between each layer of GF fabric; (b) semi-preg plies were cut and stacked on the heated tool.

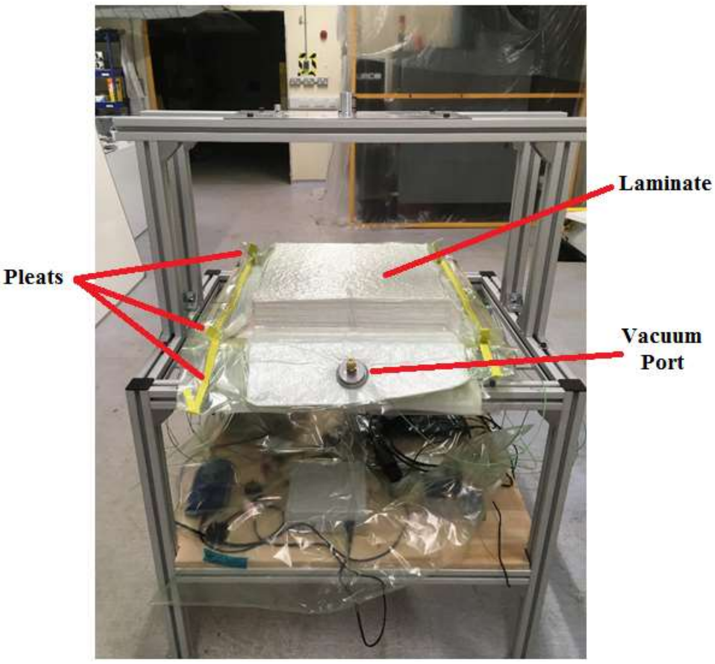

Figure 4. Photo of the laminate preform under vacuum pressure. For the insulation to fit tightly around the laminate, the vacuum bagging was pleated at the corners and an oversized pleat was used to station the vacuum port away from the laminate.

For each case, the laminates were symmetric and the ply orientation was kept constant. The plies were cut with dimensions of 400 mm × 400 mm, and were stacked at the centre of the heated tool. During the lay-up, thermocouples were placed throughout the laminates to measure temperature variations. The general positions of the thermocouples within the laminates are illustrated in Figure A.1 in Appendix A. Supplementary material. The majority of thermocouples were distributed through-thickness at the centre of the laminate, but additional thermocouples were placed towards the edge of the laminate. This arrangement of thermocouples was used to measure the through-thickness temperature variation, but also to ensure that the 1D approximation was valid for the experiment.

After laying up all of the plies and positioning the thermocouples, the vacuum bagging procedure began. For each laminate, two concentric dams of sealant tape were positioned around the laminate. The inner dam prevented excess resin flow, but contained several dry fibre tows which acted as pathways for gases to be evacuated from the laminate. In addition to this, a perforated release film was placed over the laminate to assist with air evacuation and prevent excess resin bleed. One layer of breather cloth was used as porous media for gas transport to the vacuum port. As shown in Figure 4, an oversized pleat in the breather cloth used to station the vacuum port away from the laminate so that it would not interfere with the positioning of the insulation or general heat transfer in the laminate. The vacuum bagging was pleated at the corners of the laminate to avoid obstructing the insulation i.e. the insulation sides could close over the pleats and fit tightly to the laminate using adjustable connector plates (see Figure 5).

The vacuum bagging was checked for leaks and was considered fully sealed when the vacuum pressure did not drop after several minutes. A maximum compaction pressure of approximately 85 kPa was recorded at the beginning of the tests. Measuring the thickness change due to gas evacuation was not included in this study. Instead, the initial thickness was taken as being the thickness after several minutes under vacuum. It was noted that, after applying a vacuum, Test Laminates 1 and 3 had significantly more variation in their thickness than Test Laminate 2. This was due to uneven powder dispersion which can be attributed to human error.

To avoid the accumulation of any error due to temperature effects, the LVDT support frame was designed to connect to the main tool frame such that it would not come in contact with any fixture which was subject to thermal expansion. A calcium silicate rod was used as an extension for the LVDT due to its low thermal conductivity (0.49 W/m.K) and low coefficient of thermal expansion (approximately 6.6×10^{-6} K^{-1}) [30]. This ensured that temperature correction of the LVDT sensor would not be required, and any thermal expansion of the rod would be minimal.

The LVDT took measurements from the centre of the laminate, as shown in Figure 5. The calcium silicate connecting rod was passed through a hole in the top insulation so that it came in contact with the top surface of the vacuum bagging. The LVDT's in-built spring mechanism ensured that the rod remained in contact with the surface throughout the experiment.

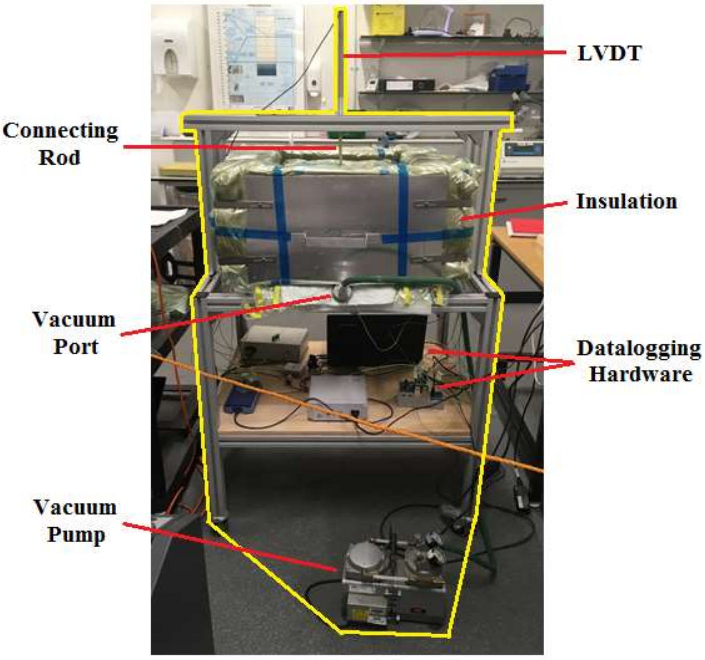

Figure 5. Photo of the apparatus (outlined in yellow) during an experiment.

2.5 Simulation of Test Laminate Processing

Process simulations of Test Laminates 1, 2 and 3 were performed using the numerical models and material properties described in Part I [16]. The initial conditions used for each simulation are given in Table 1 below. For each simulation, the ambient air temperature was assumed to remain constant at the values given in the tables. The initial temperature of the laminate, bagging, tool, etc. were assumed to be equal to the ambient temperature.

The cured ply thicknesses were determined experimentally by measuring the average thickness of single-ply laminates after being cured. The single-ply laminates were manufactured with the heated tool and vacuum pump (85 kPa compaction pressure) described in the previous sections. The manufacturer's recommended temperature cycle was used to cure the single-ply laminates.

Note that the degree of cure (DoC) for Test Laminate 1 and 3 was set to 0.2. This was because 12 months had passed between initial DSC testing of the epoxy powder [12] and manufacture of the test laminates. Repeat DSC testing showed that the DoC had increased by 0.2 while the powder was in storage (i.e. out-time effects). DSC tests were performed using a PerkinElmer DSC 8000. As in [12], a nitrogen gas purge (50 ml/min) was used with ventilated aluminium crucibles. The sample mass was an average of 9.2 mg, and a temperature ramp rate of 10°C/min was used for all tests. The influence of out-time effects on VBO prepregs have been studied by others [31,32], but further investigation was outside the scope of this work.

Table 1. Initial conditions for the simulation of all three test laminates.

Parameter [units]	Test Laminate 1	Test Laminate 2	Test Laminate 3
No. of plies	60	44	48
Cured ply thickness [mm]	0.9	1.3	1.0
Fibre volume fraction	0.5	0.5	0.45
Degree of impregnation	0.113	0.575	0.113
Powder void fraction	0.503	0.175	0.503
Degree of cure	0.2	0.01	0.2
Applied pressure [Pa]	85×10^3	85×10^3	85×10^3
Laminate/bagging/tool temperature [°C]	21	19	18

The initial degree of impregnation (DoI) for each test laminate was fitted to their initial thickness (measured by the LVDT). The initial powder void fraction of Test Laminate 2 was also fitted to the experimentally measured thickness change. In each case, the fitted values were deemed realistic – for Test Laminates 1 and 3, it was expected that powder particles would pass between fibre tows and partially fill the inter-tow region. As such, a DoI of 0.113 equates to 48% of the available inter-tow space being filled with powder when the powder void fraction is 0.503. For Test Laminate 2, the DoI was slightly more than enough to fill the inter-tow region (which was equivalent to a DoI of 0.4737), and the 0.175 void fraction accounted for any cracks in the brittle, uncured epoxy matrix, as well as gaps between the stiff semi-preg plies caused by surface roughness.

The simulations also accounted for conductive heat transfer through the insulation and the silicone rubber heating mat. Their thermal material properties are given in Table A.1.

3. Results and Discussion

3.1 Uni-directional Laminates with Epoxy Powder

The results of Test Laminate 1 are compared with simulation results in Figure 6. For Test Laminate 1, the drying cycle was split into two stages; one stage at 35°C and another stage at 55°C. At 35°C, the thickness change of laminate was negligible because the epoxy powder was below its T_g, and could not sinter. Consequently, it was clear from the temperature evolution that heat transfer was slow due to the very low thermal conductivity of the epoxy powder (assumed to be similar to the thermal conductivity of polyamide powder – approximately 0.075 W/m K [33,34]). By comparison, the rate of heat transfer improved in the second stage of drying at 55°C. This was because the powder began to sinter, and the laminate thickness decreased significantly. The sintering model captured the general trend of the thickness decrease but lacked accuracy in describing the temperature dependence of the epoxy powder w.r.t. sintering. This inaccuracy was most likely related to poor temperature control and pressure-dependent effects during the parallel-plate rheometry tests described in Part I [16]. It may be improved by repeating tests with a temperature-controlled test chamber and varying the applied pressure or, alternatively, using thermomechanical analysis (TMA) [35].

In terms of the heat transfer model, the simulation was accurate throughout, except for a slight underestimation of the temperature increase at the centre of the laminate during the drying and impregnation stages (approximately 3°C); most likely due to the inaccuracy of the sintering model. Both experiment and simulation showed that the exothermic curing reaction increased the rate of temperature change, but did not result in any thermal overshoot of the programmed temperature cycle.

The experimental and simulated thickness change data (Figure 6(b)) converged during the impregnation stage as the powder finished sintering and resin flow became the dominant process. The resin flow model predicted a distinct transition from inter-tow flow to intra-tow flow – identified by a sudden change in slope for the thickness change curve, midway through the impregnation stage – however, this transition was not distinguishable in the experimental data. This suggested that, in reality, fabric impregnation was characterised by a more gradual transition between the two flow domains. This type of transitional flow has been modelled for liquid resin infusion (LRI) processes, such as resin film infusion, using the Brinkman equation [36]. Although inter-tow flow in VBO prepregs occurs over a much smaller scale than LRI processes, use of the Brinkman equation may improve the accuracy of simulating this transition in future work.

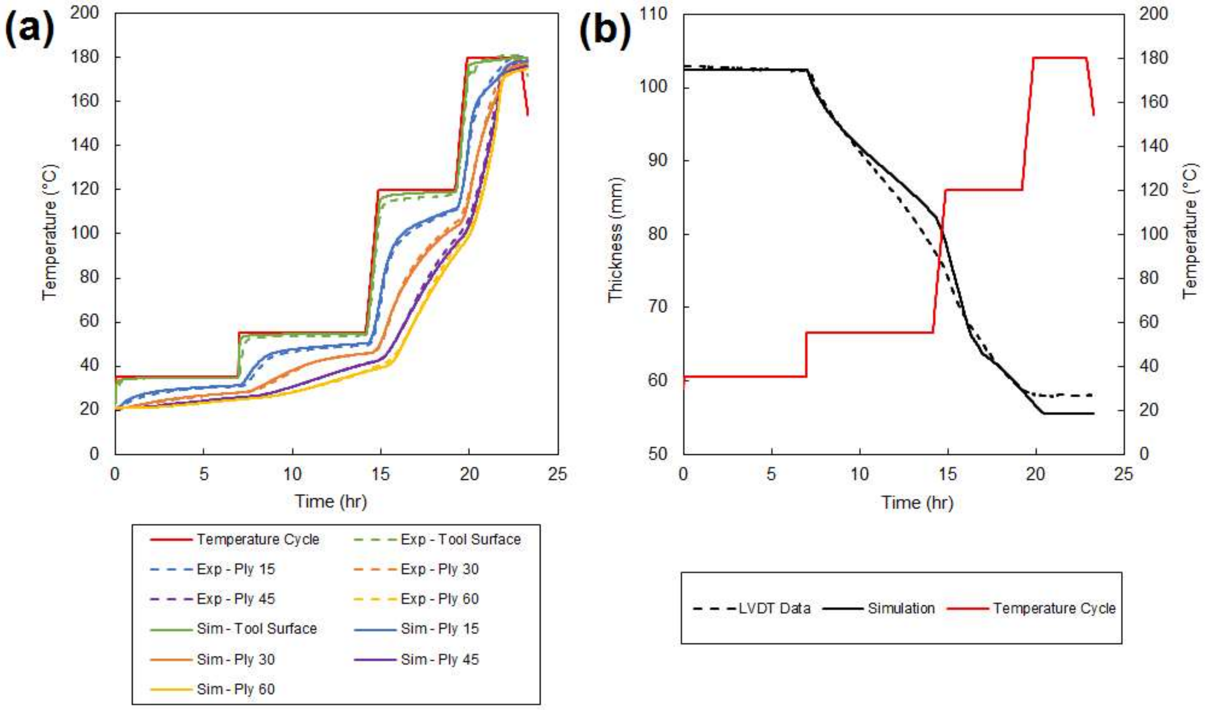

Figure 6. Comparison of simulations and experimental results for Test Laminate 1: (a) the simulated temperatures accurately matched the thermocouple data; (b) the simulated thickness change captured the overall trend of the LVDT data, however, there was some inaccuracy in the sintering model and in the prediction of the final thickness.

The simulation also predicted an abrupt plateau in thickness change after 20 hr, signalling the end of resin flow, whereas the experiment showed a more gradual cessation. It was found that the simulation overestimated the total thickness change by approximately 2.5 mm. Cender *et al.* [19] noted similar mismatch between experiment and simulation at higher DoI, and attributed it to resin-fibre pressure sharing. More recently, Helmus *et al.* [21] have developed models for VBO prepregs which can account for fibre bed compaction (due to gas evacuation) and resin-fibre pressure sharing during impregnation. Similar models could be developed to describe the material system presented here, but were outside the current scope of work.

Figure 7. Cut-section of Test Laminate 1 showing the non-uniformity of thickness due to manual powder dispersion.

Centea and Hubert [20] found that reduced vacuum or restricted evacuation resulted in an increased void content for laminates manufactured using VBO prepregs, and that it had an effect on the rate of thickness change of the laminate. Using the same experimental apparatus developed by Centea and Hubert [20], Helmus *et al.* [21] showed pressure deficient conditions resulted in a more gradual plateauing of experimentally measured thickness change. Despite their model accounting for compaction and resin-fibre pressure sharing, they presented a similar mismatch between simulation and experiment as what was seen in Figure 6(b). To assess the mismatch in Figure 6(b) further, a section was cut from Test Laminate 1 and the interior of the laminate was inspected (see Figure 7). It was noted that Test Laminate 1 had a relatively uneven thickness (± 6.8% variation) due to the manual dispersion of powder between the plies. Microscopic inspection confirmed that resin rich areas resulted in undulations in the fabric, and revealed that partially dry fibre tows, as well as inter-tow voids, were widespread in the upper third of the laminate. In addition to this, sporadic incomplete tow impregnation was visible in the lower two thirds of the laminate. Figure 8(a) shows the general defects that formed in the upper third of the laminate, while Figure 8(b) shows the intra-tow voids at the centre of the tows under increased magnification. The void dispersion within the upper third of the laminate displayed no obvious gradient, and may be as a result of deficient pressure (due to poor vacuum and/or entrapped gas). The incomplete tow impregnation in the remainder of the laminate may be due to resin-fibre pressure sharing effects also [19].

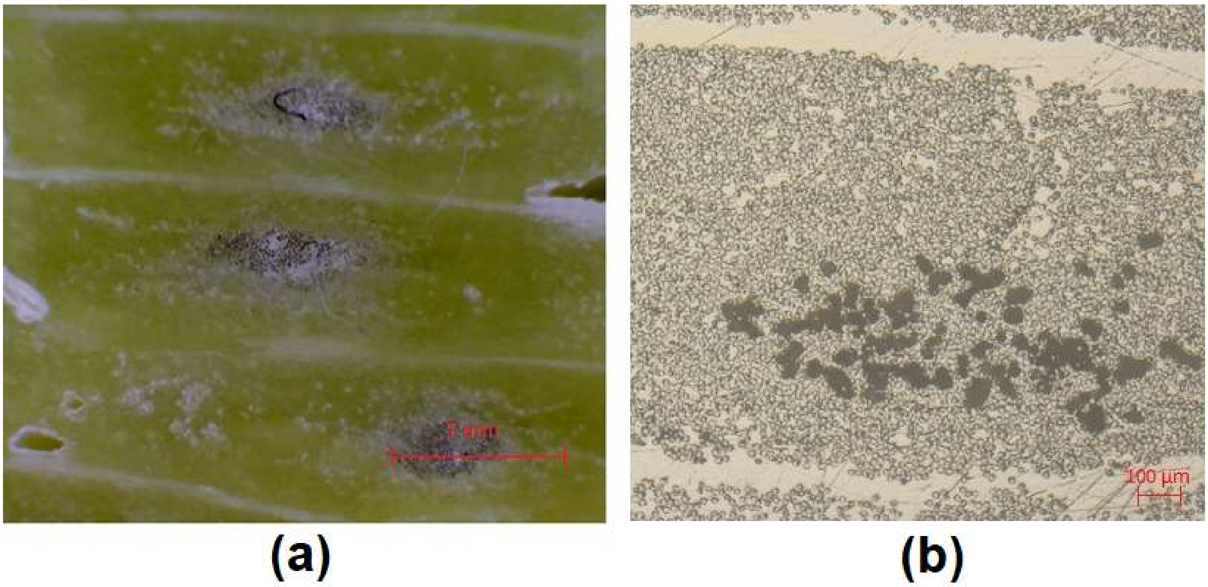

Figure 8. Microscope images of Test Laminate 1: (a) both incomplete tow impregnation and inter-tow voids are visible in the upper third of the laminate (X1 magnification); (b) the image reveals the intra-tow voids at the centre of the tow caused by incomplete impregnation (X5 magnification).

Additional checks were performed to identify potential sources of experimental error. It was found that thermal expansion effects were negligible for Test Laminate 1 (± 3% of the total thickness change), and that a temperature difference did exist between the centre and edges (maximum of 13.5°C, but generally < 10°C), but the through-thickness temperature difference was large enough (maximum of 80°C) to dominate heat transfer within the laminate. These checks are discussed further in Appendix A. Supplementary material.

For Test Laminate 3, efforts were made to reduce sources of error (i.e. void formation, in-plane temperature difference, etc.). In the case of void formation, it was hypothesised that Test Laminate 1 contained resin starved regions which may have been alleviated by increasing the resin content for Test Laminate 3, however, the change had little or no effect. One potential reason for this is that a maximum compaction pressure of 85 kPa was achieved for each test due to limitations with the vacuum pump. Ideally, up to 101 kPa should be achieved for VBO processes, as it has been shown that pressure deficient conditions can result in up to 5.5% voids in thin laminates made from VBO prepregs [20]. This could suggest that Test Laminates 1 and 3 suffered from pressure deficient conditions, despite careful checks for vacuum leakage. More experiments and analysis are required to investigate this further, however, this outside the scope of the current work.

Another possibility is that the epoxy powder may have been subject to greater ‘out-time’ effects than what was expected, which can have significant consequences for the tow impregnation and porosity in the cured laminate [32,37]. In particular, Grunenfelder *et al.* [32] showed that tow impregnation of conventional VBO prepregs was inhibited by a significant increase in resin viscosity (two orders of magnitude) for 56 days of out-time.

In either case, the formation of these defects was not predicted by the process simulations and forms an obvious area of improvement for future development of the simulation tools.

3.2 Partially Impregnated Triaxial Laminate

As previously mentioned, Test Laminate 2 differed from the other test laminates in that it was a stitched triaxial fabric which had been partially impregnated with GRN 918 in an automated process. This meant that the powder dispersion was more uniform, and that the thickness change due to sintering was expected to be much less for the laminate.

The experimental data for Test Laminate 2 is compared against the results of the 1D simulations in Figure 9. The finite difference code was adjusted to account for resin flow into the three layers of fibre tow in the triaxial fabric. The simulations were again accurate in capturing the general processing behaviour of the test laminate, however, in this case, the simulation slightly underpredicted the temperature increase during the impregnation and curing. This may have been related to a difference in the through-thickness thermal conductivity of the triaxial fabric, or because of the lower void content of the laminate (discussed further at the end of this section). It was noted that the Test Laminate 2 had better in-plane temperature uniformity than Test Laminates 1 and 3 (< 5°C in-plane temperature difference, see Figure A.5 in Appendix A. Supplementary material). As such, greater confidence could be taken from the 1D heat transfer approximation.

Another interesting feature of Figure 9(a) was that the temperature increased faster during the drying stage due to thermal conductivity of the sintered epoxy being approximately 120% higher than the powder, and the reduced initial thickness. The top ply of Test Laminate 2 reached 40°C after 5.66 hr, whereas Test Laminate 3 took 9.16 hr to reach 40°C. Bearing in mind the advantages of drying the epoxy in powder form (i.e. high surface area for desorption of moisture, and higher permeability [38,39]), this result showed that there was an obvious trade off in processing advantages between the two material forms.

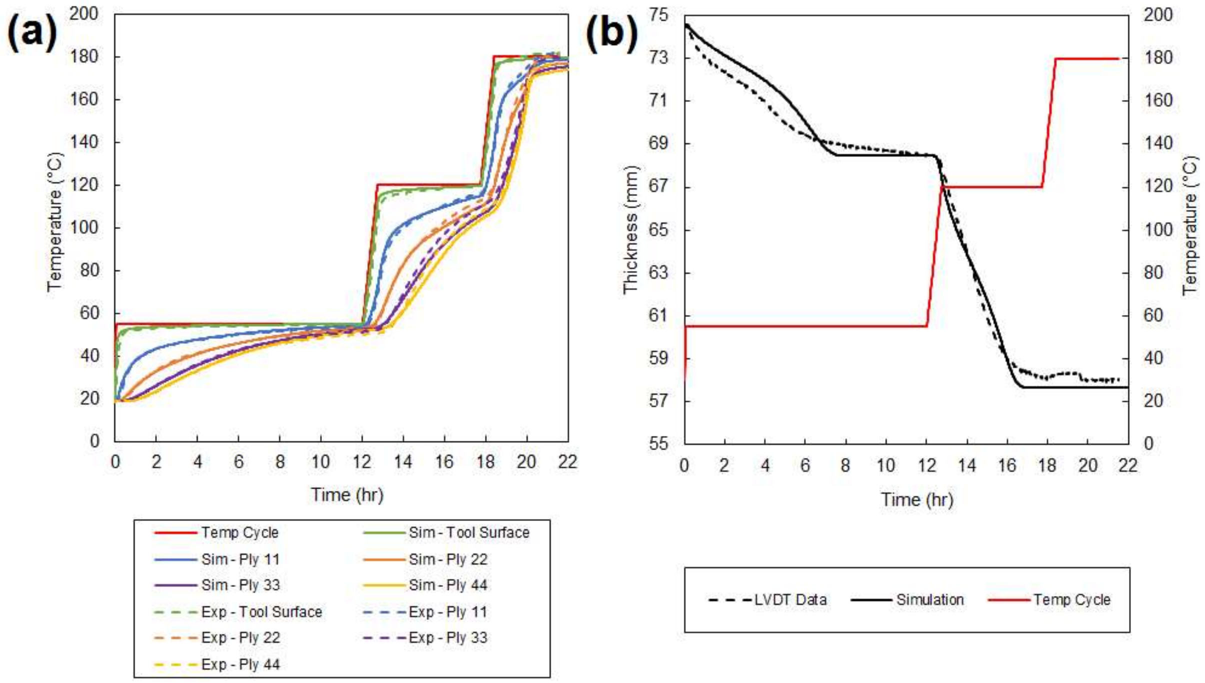

Figure 9. Comparison of simulations and experimental results for Test Laminate 2: (a) the simulated temperatures accurately matched the thermocouple data; (b) LVDT data shows that although the epoxy powder had been fully sintered during the production of the VBO prepreg, the thickness of the laminate still reduced by several millimetres.

In terms of the LVDT data (Figure 9(b)), it was interesting to note that, despite the epoxy being fully sintered in the VBO prepreg production process, Test Laminate 2 was still compacted by several millimetres during the drying stage. To account for this, the simulation was given an initial powder void fraction of 0.175. Most likely, there were two sources for the initial void fraction: (1) the formation of cracks in the brittle uncured epoxy matrix during handling, and (2) the formation of gaps between the stiff, board-like plies during lay-up.

As shown in Figure 10, Test Laminate 2 had much better thickness uniformity (variation of ± 1%) than the other laminates. It also seemed to have much less visible defects, however, optical microscopy of the cut-section (see Figure 11) revealed that there were cases of sporadic incomplete tow impregnation and larger inter-tow voids. The latter case was particularly true in the mid-plane of the laminate where prepreg plies had been stacked symmetrically so that their resin rich surfaces were in contact. Given the fully sintered form of the epoxy, this was possibly a result of entrapped gases, as air and water vapour would have had more resin to pass through in order to reach a dry fibre pathway for evacuation. The sporadic incomplete tow impregnation may have been due to resin-fibre pressure sharing [19].

Although the void content of the laminates was not quantified, the difference in void content was noticeably higher for Test Laminates 1 and 3 based on visual inspection. In terms of the heat transfer model underpredicting the temperature increase in Test Laminate 2, it was possible that the higher void content of Test Laminates 1 and 3 corresponded with lower thermal conductivity, as was the case with the powder void fraction. The thermal conductivities for simulations may be manually adjusted for differences in void content, but ideally a suitable model would be added to the numerical code which can account for such behaviour.

Figure 10. Cut-section of Test Laminate 2.

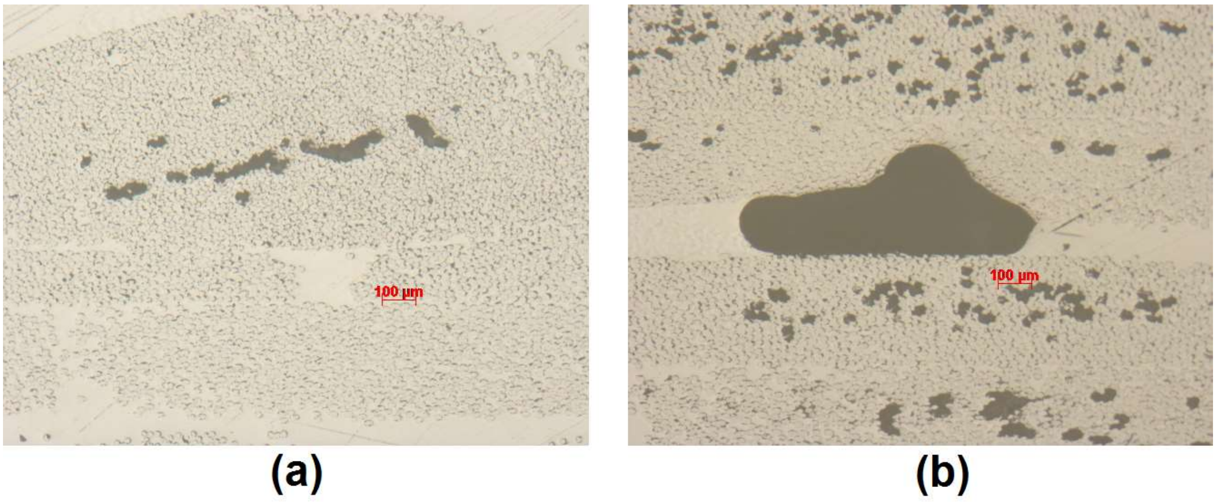

Figure 11. Micrographs of Test Laminate 2 at two locations. (L) Intra-tow voids caused incomplete tow impregnation. (R) Inter-tow and intra-tow voids caused by gases which were entrapped at the laminate midplane (i.e. plane of symmetry).

3.3 Investigation of VBO Prepreg Format

With the simulations validated for two different VBO prepreg formats, it was worthwhile considering the advantages and disadvantages of each format in more detail. From dynamic vapour sorption (DVS) analysis, it was known that as-supplied epoxy powder performed significantly better w.r.t water desorption when compared to sintered epoxy [38]. Furthermore, it was hypothesised that it would improve the through-thickness gas permeability of the VBO prepreg compared to a format with homogenous resin layers. On the other hand, epoxy powder increased the initial thickness of the laminate preform by up to 30% and had a thermal conductivity which was 55% lower than that of fully sintered epoxy. To determine the severity of this effect on heat transfer, the 100-ply GF/Epoxy-powder case study from Part I [16] was repeated with three different initial values of powder void fraction. As in Part I [16], the laminate was given forced convection boundary conditions with a heat transfer coefficient (HTC) of 40 W/m^{2}K. The remaining initial conditions are given in Table A.2 in Appendix A. Supplementary material. Figure 12 shows the temperature plots for Ply 50; the ply most affected by this phenomena i.e. at the centre of the laminate, furthest from the heat source. The results showed that only the drying stage was affected by the powder format, and that the effect diminished as the powder sintered. Given this relatively small impact on heat transfer, the advantages of a powdered format may outweigh the advantages of a fully sintered VBO prepreg.

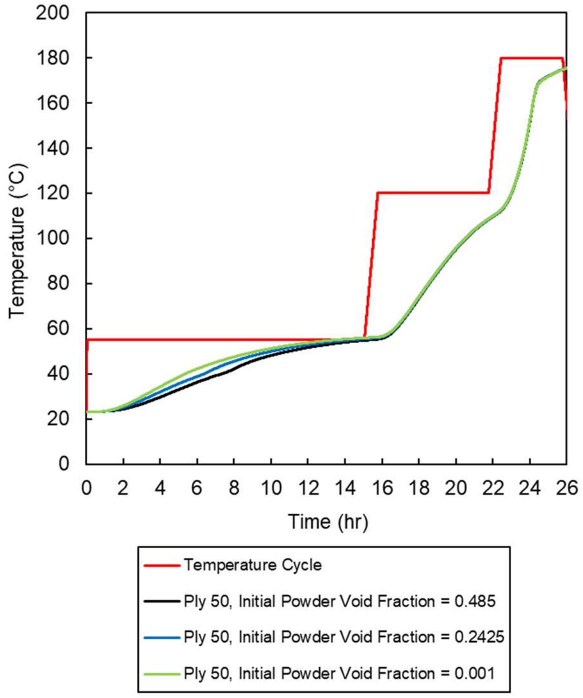

Figure 12. Plot of the temperature at Ply 50 for varying levels of initial powder void fraction.

3.4 Investigation of Thickness Effects

The relatively small effect of the powder void fraction w.r.t. heat transfer suggested that perhaps the coupling of heat transfer and thickness change was not as important as previously considered. To verify whether coupling these effects was necessary or not, another simulation of the 100-ply laminate was run for a fully consolidated laminate (i.e. fully sintered and infused).

As can be seen in Figure 13, there were relatively significant discrepancies between the two simulations during the drying and impregnation stages, while the solutions converged during the cure stage. The effect was more pronounced than in Figure 12 because the thickness change due to impregnation, as well as sintering, was unaccounted for in the fully consolidated case. Naturally, these discrepancies influenced other processes like fabric impregnation and cure evolution. As such, the importance of coupling the models for powder-based VBO prepregs was verified. In contrast, this effect was less prominent for the semi-preg used in Test Laminate 2, so decoupling could be possible for this format without a significant loss of accuracy in the simulated results.

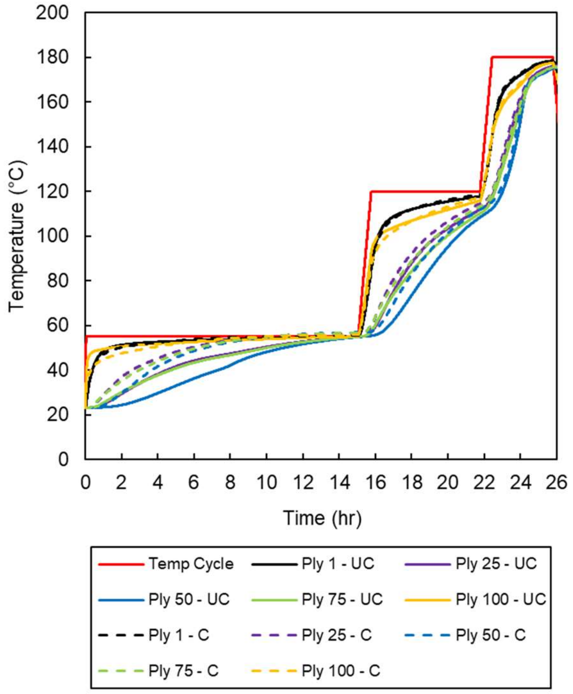

Figure 13. Comparison of simulations for a consolidated (C) laminate and an unconsolidated (UC) laminate. The consolidated laminate simulation assumed a constant thickness throughout.

3.5 Investigation of Heating Methods

Two sets of heating methods were considered for this work; heated moulds/tooling (specified temperature BCs), and oven heating (forced convection BCs). Heated moulds are common for manufacturing large parts, such as wind turbine spars, root section, skins, shear webs, etc., because they are inexpensive compared to purchasing and operating very large ovens. For processing thick-section parts, however, heated moulds can be inefficient as they typically only provide one-sided heating. Looking at the heat equation (Equation 1), the conduction term in the equation is dependent on the second spatial derivative of temperature.

$$\rho_c c_{P,c} \frac{\partial T}{\partial t} = \kappa \nabla^2 T + (1 - V_f)\rho_r H_T \frac{\partial \alpha}{\partial t} \tag{1}$$

Where ρ_c is the composite density [kg/m^3], $c_{P,c}$ is the specific heat capacity of the composite [J/kg K], T is temperature [K], κ is anisotropic thermal conductivity [W/m K], V_f is the fibre volume fraction, ρ_r is the resin density [kg/m^3], H_T is the total enthalpy of the curing reaction [J/g], and α is the DoC.

By halving the distance that the heat must transfer, the rate of change for temperature can be greatly increased. This effect can be seen in Figure 14, which shows that processing of the 100-ply laminate was significantly faster for two-sided heating. This was also evident from the temperature plots, Figure A.6 and Figure A.7, which are given in Appendix A. Supplementary material. Due to the low exotherm of the epoxy powder, two-sided heating can be used with this system to significantly reduce the processing time of thick sections.

Figure 14 also shows the results of a third arrangement which combined heated tooling with the use of silicone rubber heating mats on the top surface of the laminate. The aim of this additional arrangement was to explore an alternative method for two-sided heating which might achieve a lower capital cost than oven heating. For manufacturing a real, 3D geometry, the concept would be to use the heating mats only in areas of increased thickness as one-sided heating is sufficient for thin structures. Highly flexible, silicone rubber heating mats are available [40] which could conform to the shape under a double vacuum bagged arrangement i.e. the heating mat could be placed between two vacuum bags.

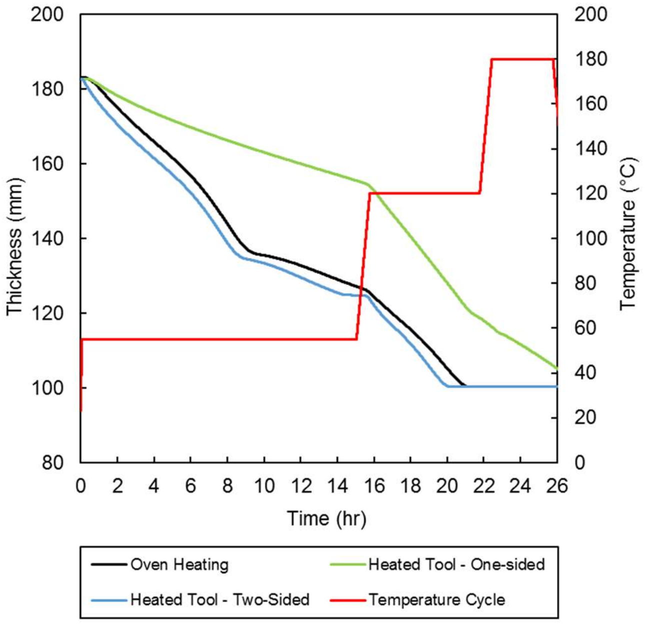

Figure 14. Simulated consolidation of three 100-ply laminates manufactured using different thermal boundary conditions. Consolidation was significantly slower for one-sided heated tooling when compared to two-sided heated tooling or oven heating (also two-sided heating).

3.6 Methods for Reducing Thermal Gradients and Cure Gradients

As previously discussed, one of the main challenges with processing thick-section composite laminates is the development of large thermal gradients and cure gradients due to the highly exothermic nature of conventional thermoset systems. It is known that epoxies undergo chemical shrinkage due to increases in molecular density during polymerisation and crosslinking [41]. This shrinkage can create mismatches in volume within the composite structure, which can be "locked-in" as the elastic modulus of the epoxy develops above the gel point [42]. Consequently, residual stresses can develop and lead to warpage or matrix micro-cracking [10].

In the case of a 100-ply laminate processed in an oven, the overall duration of gelation may last for hours, as shown in Figure 15(a). While the use of epoxy powder can eliminate thermal overshoot as a processing hazard, Figure 15(b) shows that large peaks in the temperature and cure difference occur throughout the recommended processing cycle. Moreover, peaks in both temperature difference and in DoC difference overlap with the period of gelation in the laminate.

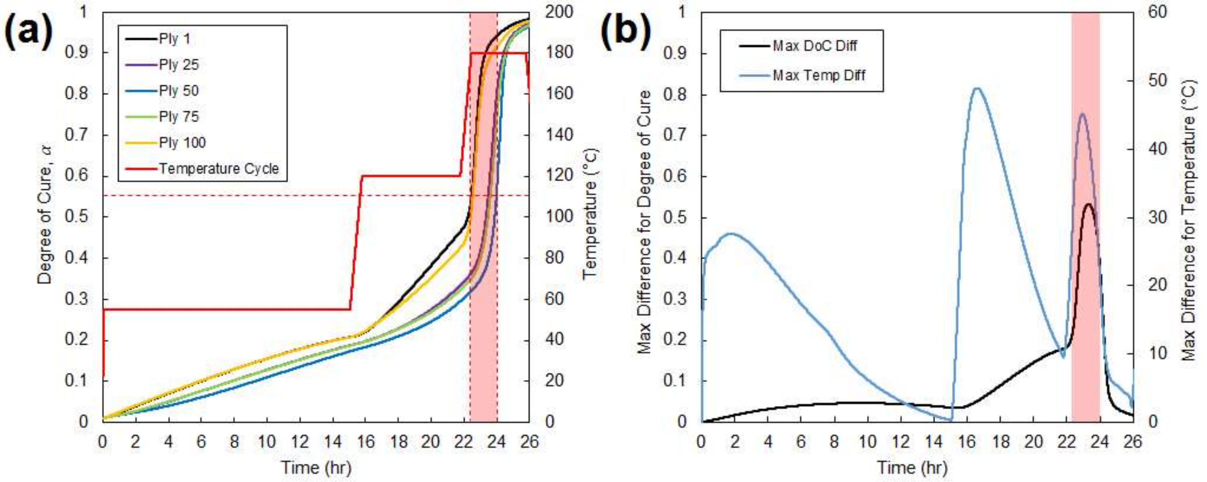

Figure 15. (a) Simulated DoC evolution for the 100-ply laminate of UD GF/GRN 918. The horizontal dashed red line represents the gel point ($\alpha_g = 0.56$ [12]), while the shaded red area shows the timespan of gelation in the laminate. (b) Plot of the maximum DoC difference and the maximum temperature difference. The peaks in the max differences overlap with gelation of the laminate, meaning that any corresponding residual stresses would be locked in.

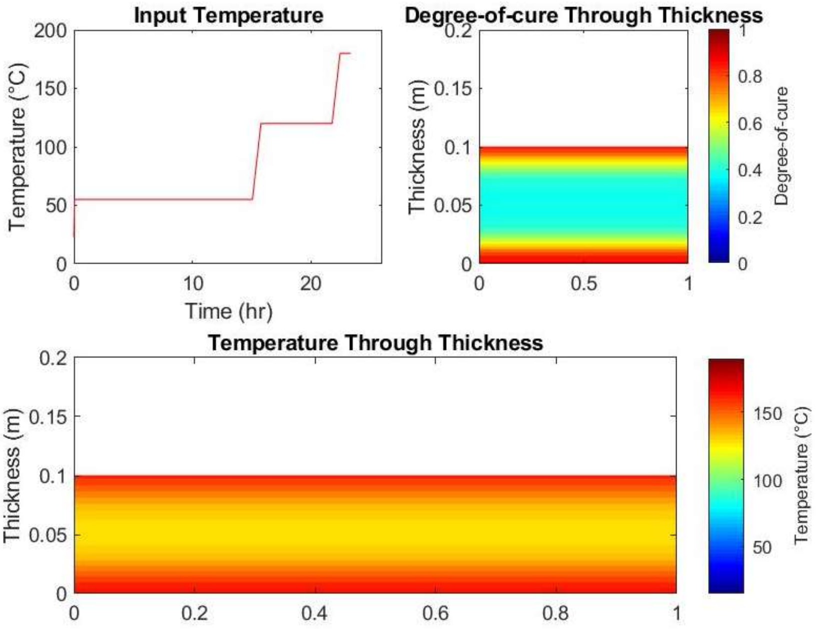

Figure 16. Simulation results at approximately 23.3 hr into the temperature cycle. Large cure gradients are predicted between the outside and inside of the laminate; indicated by the colour contour (top right). This coincides with temperature gradients within the laminate, corresponding to a temperature difference of 40°C between the surface and the centre of the laminate (bottom)

Another important factor to consider is that, when the cure difference is highest (23.3 hr into the cycle), the outside of the laminate is above the gel point and the inside of the laminate is not. In effect, this would create a hard outer shell that resists further shrinkage within the laminate's core [41]. This outside-to-inside curing (shown in Figure 16) is considered undesirable due to the potential for large tensile and compressive stresses in the inside and outside of the laminate, respectively. Bogetti and Gillespie [10] showed that these stresses are enough to initiate transverse matrix cracking in GF/Polyester laminates. Note – a full video of the simulation is available in Appendix A. Supplementary material; see Video 1.

The outside-to-inside curing profile is related to the cure kinetics of the epoxy powder. Above 120°C, the cure rate of the outer plies increases rapidly due to activation of the latent curing agent, while the central plies lag due to the low enthalpy of reaction. For a standard epoxy system this would not normally happen as the resin at the centre of the laminate generates sufficient heat to auto-accelerate the curing; commonly resulting in an inside-to-outside cure profile [10].

Ultimately, without developing a residual stress model, it was impossible to know the implications of the outside-to-inside curing shown in Figure 16. Nevertheless, it was worthwhile to investigate how the gradients can be reduced. One concept was the use of a second epoxy powder with cure kinetics that differ from GRN 918 e.g. lower or higher heat activation temperature than GRN 918. By distributing the “lower activation temperature” epoxy powder at the centre of the laminate, and the “higher activation temperature” epoxy at the outside of the laminate, it was expected that curing could be partially synochronised across the thickness of the laminate. This concept was formed on the basis that the epoxies maintained their global position within the laminate because each layer only flowed through-thickness into the adjacent fabric layer. For other VBO processes, such as VARTM, such an arrangement would not be possible because it would be impossible to control the through-thickness distribution of the resins during infusion.

To test this concept, the cure kinetics of a “higher activation temperature” epoxy powder were approximated using an existing cure kinetics model developed for epoxy powders [12]:

$$\frac{d\alpha}{dt} = \frac{(k_{\alpha 1} + k_{\alpha 2} + k_{\alpha 3}\alpha^m)(1-\alpha)^n}{1 + \exp[C(\alpha - \alpha_c)]} \tag{2}$$

Where $k_{\alpha 1}$, $k_{\alpha 2}$, and $k_{\alpha 3}$ are cure rate constants [s^{-1}], m and n are the reaction orders, C is a diffusion constant, and α_c is the temperature-dependent critical DoC, above which the reaction becomes diffusion-controlled.

HZH01R – an epoxy powder from AkzoNobel which was previously investigated for use in composites manufacturing [12] – was used as the basis for the “higher activation temperature” epoxy powder. The corresponding cure kinetics parameters are given in Table 2. Note, full characterization of the parameters was not performed, and the given values were simply used as first approximation for proof of concept. For the modified laminate simulation, HZH01R is placed between plies 1 and 24 and between plies 75 and 100. GRN 918 is placed between plies 25 and 74 because it had a lower activation temperature.

Another means of reducing the thermal gradients and cure gradients was modification of the temperature cycle. Although, optimisation algorithms have previously been developed for the processing of thick-section composites [43–45], the development of such algorithms were outside the scope of this project. Nevertheless, it was possible to manually run simulations for several iterations of the temperature cycle. As such, the optimization of temperature cycle was performed by minimizing $\Delta\alpha$ and ΔT during gelation, while ensuring that full fabric impregnation was achieved prior to gelation. It was assumed that residual stress development would begin at the gel point (i.e. DoC = 0.56) and that the effects of any gradients prior to gelation were negligible [42]. In addition, it was decided that the drying stage could be cease as soon as the powder was fully sintered, as any further desorption of moisture would be negligible.

Table 2. First approximation of cure kinetics parameters for HZH01R.

Parameter [unit]	Value	Parameter [unit]	Value
A_1 [s^{-1}]	4.073 × 10^{-4}	m	1.24
E_1 [J/mol]	12006	n	1.8
A_2 [s^{-1}]	7.359× 10^{12}	C	50
E_2 [J/mol]	137594	α_c	0.006 T - 1.748
A_3 [s^{-1}]	1.097× 10^{13}		
E_3 [J/mol]	131251		

The optimised cycle (performed manually) was as follows:

- Drying stage: Ramp to 55°C and hold for 540 min
- Impregnation stage: Ramp to 135°C at 1.5°C/min and hold for 480 min
- Cure stage: Ramp to 180°C at 0.25°C/min and hold for 300 min

Figure 17 shows the simulated temperature distribution when two powders are used in combination with an optimised temperature cycle. The drying stage was significantly shorter than the recommended cycle, while the impregnation stage was longer. By increasing the temperature and duration of the impregnation stage, the ply temperatures could converge prior to the start of the cure stage. This temperature convergence was aided by the heat being generated from the curing reaction at the centre of the laminate; allowing the temperature of the inner plies to approach the temperatures of the outer plies. The slower ramp to the final curing temperature meant that the temperatures did not diverge significantly for the remainder of the temperature cycle, thus minimizing the thermal gradients.

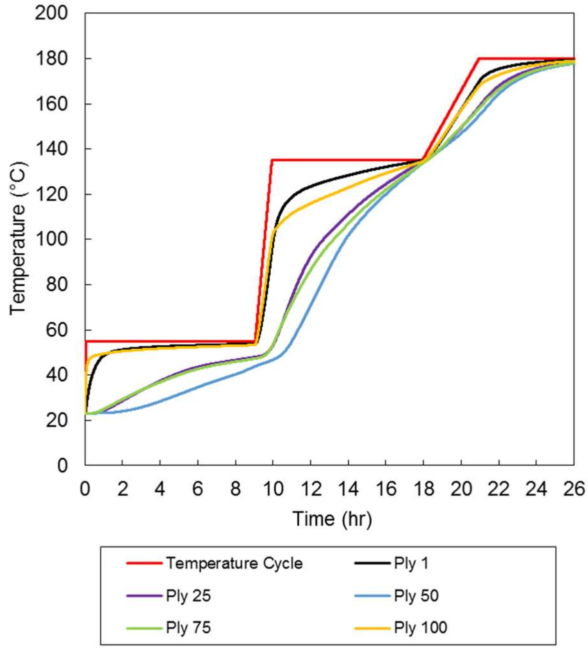

Figure 17. Plot of simulated temperatures for modified laminate and temperature cycle.

Figure 18(a) shows the effect of the two modifications on the DoC evolution. The cure rate at the centre of the laminate (i.e. Ply 50) was faster than the cure rate at Ply 75 during the impregnation stage (after approximately 14 hr). This was because GRN 918 (plies 25 to 74) has a lower heat activation temperature compared to HZH01R (plies 1 to 24, and plies 75 to 100). Despite the period of gelation being increased, by activating the latent curing agents in the epoxy at the centre of the laminate, the maximum DoC difference could not grow as large as what it was in the standard 100-ply laminate. It was also noted that the fabric impregnation had completed after approximately 14 hr. Figure 18(b) highlights the improvements achieved via the modified laminate and temperature cycle. The period of gelation in the laminate (identified by the red shaded area) overlapped with a trough in max temperature difference, and the peak in max DoC difference was reduced from 0.53 to 0.28. One potential area of concern with using two epoxy powders, was that it could cause large localized gradients of DoC at the interface of the two epoxies (this can be seen in the simulation video – see Video 2 in Appendix A. Supplementary material). This risk may be reduced by mixing powders so that the transition from one powder to the other is more gradual, however, the epoxies would need to be compatible so that they do not create a region with poor interlaminar properties.

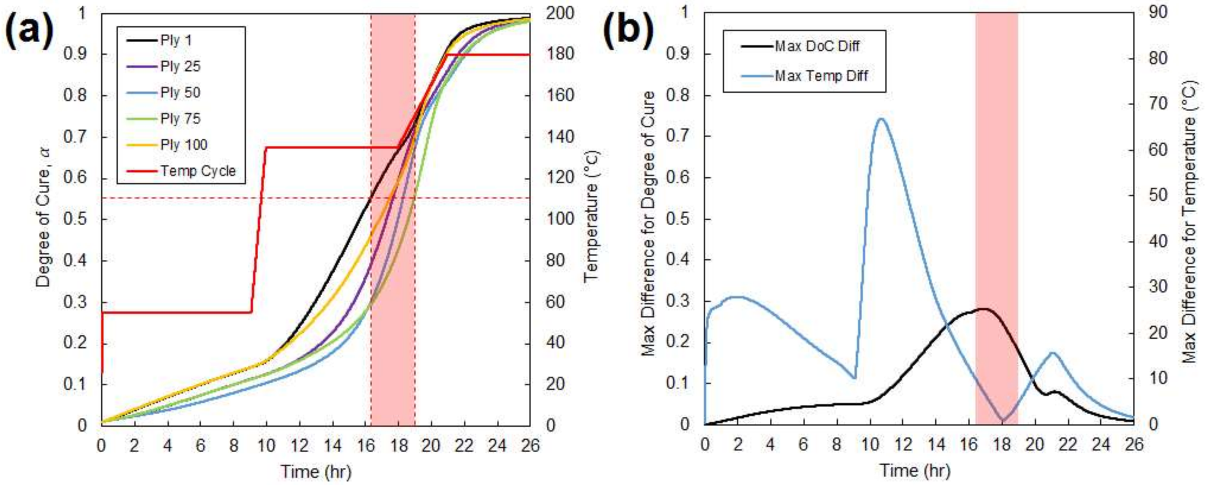

Figure 18. (a) DoC evolution for the modified laminate and temperature cycle. The horizontal dashed red line denotes the gel point ($\alpha_g = 0.56$ [12]), and the shaded red area outlines the period of gelation within the laminate. (b) Maximum DoC difference and maximum temperature difference for the modified laminate and temperature cycle. While the peak in max DoC difference still occurred during gelation, it was reduced significantly with the introduction of another epoxy powder.

The manually optimized temperature cycle was also run for a 100-ply thick laminate which only contained GRN 918 as the polymer matrix, the results of which are given in Figure A.8 and Figure A.9 in Appendix A. Supplementary material. The modified cycle also reduced the max temperature difference in this case, however the effect on DoC was less pronounced without the use of a second epoxy powder.

4. Conclusions

Experimental validation of 1D process models for epoxy powder VBO prepregs has been presented. Three test laminates were manufactured – Test Laminates 1 and 3 were manufactured using uni-directional glass-fibre (UD GF) fabric with epoxy powder (GRN 918) manually dispersed between plies, and Test Laminate 2 was manufactured using triaxial GF fabric which was partially impregnated with GRN 918 in an automated prepregging process.

Temperature measurements for Test Laminate 1 and 3 showed that epoxy powder inhibited heat transfer through thick sections due to its low thermal conductivity. In contrast, Test Laminate 2 showed that by sintering the powder during the prepregging process, heat transfer was improved significantly during the initial drying process. The relationship between heat transfer and the initial powder void fraction was confirmed with additional simulations. This has implications for manufacturing thick-section structures with this material system because it is already difficult to heat thick-sections due to the relatively low through-thickness thermal conductivity of the fibre reinforcements. Nevertheless, the powder form of the epoxy may also possess important processing benefits, including better sorption properties and better through-thickness permeability for evacuating gases during the drying stage of the process. In conclusion, further analysis and modelling is required to understand the effect of the VBO prepreg format on moisture desorption and gas evacuation during the drying stage.

Another significant difference between the test laminates was the importance of the automated powder dispersion used in the prepregging process. Manual dispersion of the powder was labour intensive, made material handling difficult, and was prone to uniformity due to human error. This resulted in uneven laminate thicknesses for Test Laminates 1 and 3, whereas Test Laminate 2 had much greater uniformity. It may possible to manufacture prepreg with partially sintered powder which handles better and produce better laminate uniformity, but this requires more development with prepreg manufacturers.

In terms of validation, the experiments showed that the process models developed in Part I [16] captured the general behaviour of the material system during VBO processing. Thickness measurements confirmed large bulk reduction due to powder sintering as well as resin flow, however, some discrepancies were identified for the models describing these processes. Cut-sections of the cured test laminates revealed inter-tow and intra-tow voids. These voids were thought to be a result of a combination of entrapped gases, resin-fibre pressure sharing, and possibly out-time effects which weren’t captured by the current models. To better describe the resin flow within the material system, more complex models are required to describe the transition from inter-tow flow to intra-tow flow [36], and resin-fibre pressure sharing [21]. Similarly, further development could include investigations into gas evacuation and out-time effects. It is expected that further characterisation of the sintering process would produce more accurate semi-empirical parameters for the model that was developed.

The heat generation due to cure, and heat transfer in general, was accurately predicted by the heat transfer and cure kinetics models. Both the experiments and the simulations confirmed that thick laminates manufactured using epoxy powder do not exhibit any significant thermal overshoot. After further investigation, however, it was found that large temperature differences and degree of cure (DoC) differences developed through the thickness of the laminate when using the manufacturer’s recommended temperature cycle. For a 100-ply thick laminate, peaks in differences overlapped during gelation within the laminate. It was considered that this occurrence would put the laminate at risk of developing large residual stresses due to mismatches in thermal expansion and chemical shrinkage. The implication of this was that the residual stresses could cause part warpage and/or matrix micro-cracking. While no evidence of either was found for the three test laminates, residual stress development should be modelled as part of future work so that it can be understood how the processing affects the final stress state of the cured laminate. This is necessary because thick-section laminates are typically used for load bearing structures, such as the root of a wind turbine blade; the mechanical performance of which may be affected by its initial process-induced stress state.

In the absence of a residual stress development model, a modified laminate lay-up and temperature cycle were proposed to reduce the differences in temperature and DoC. The modifications resulted in the temperature difference reaching a minimum during gelation, and a 47% reduction in the maximum DoC difference. This suggested that the processing of thick-section structures with epoxy powder could be optimised not only by modifying the temperature cycle, but also by locally varying the latency of the powder given that the resin flow occurs over a small length scale. The potential for this modifiable feature has yet to be explored experimentally but may be of interest for future work. An additional concept for locally heating thick-sections, using flexible heating mats, was also simulated. This concept could be used as a means of achieving two-sided heating at a reduced cost compared to oven heating. As this material technology has primarily been developed for renewable energy applications, this concept could be explored industrially as a means of reducing turbine blade manufacturing costs, and thereby reducing the levelised cost of energy for wind and tidal energy.

Acknowledgements

The authors acknowledge financial support from MARINCOMP, “Novel Composite Materials & Processes for Marine Renewable Energy”, a European Union Marie Curie FP7 Project funded under the IAPP call (Grant No. 612531) and industrial partners Suzlon Energy Limited (NL Branch), Johns Manville, and ÉireComposites Teo. We also acknowledge funding from POWDERBLADE, “Commercialisation of Advanced Composite Material Technology: Carbon-Glass Hybrid in Powder Epoxy for Large Wind Turbine Blades”, funded under: European Union Horizon 2020, Fast Track to Innovation Pilot, Grant No. 730747.

References

[1] Garschke C, Weimer C, Parlevliet PP, Fox BL. Out-of-autoclave cure cycle study of a resin film infusion process using in situ process monitoring. Compos Part A Appl Sci Manuf 2012;43:935–44. https://doi.org/https://doi.org/10.1016/j.compositesa.2012.01.003.

[2] Hardis R, Jessop JLP, Peters FE, Kessler MR. Cure kinetics characterization and monitoring of an epoxy resin using DSC, Raman spectroscopy, and DEA. Compos Part A Appl Sci Manuf 2013;49:100–8. https://doi.org/https://doi.org/10.1016/j.compositesa.2013.01.021.

[3] Lionetto F, Moscatello A, Maffezzoli A. Effect of binder powders added to carbon fiber reinforcements on the chemoreology of an epoxy resin for composites. Compos Part B 2016;112:243–50. https://doi.org/https://doi.org/10.1016/j.compositesb.2016.12.031.

[4] Oh JH, Lee DG. Cure Cycle for Thick Glass/Epoxy Composite Laminates. J Compos Mater 2002;36:19–45. https://doi.org/https://doi.org/10.1177/0021998302036001300.

[5] Kratz J, Hsiao K, Fernlund G, Hubert P. Thermal models for MTM45-1 and Cycom 5320 out-of-autoclave prepreg resins. J Compos Mater 2012;47:341–52. https://doi.org/https://doi.org/10.1177/0021998312440131.

[6] Shi L. Heat Transfer in the Thick Thermoset Composites. PhD Thesis, Technische Univeristeit Delft, 2016.

[7] Loos AC, Springer GS. Curing of Epoxy Matrix Composites. J Compos Mater 1983;17:135–69. https://doi.org/https://doi.org/10.1177/002199838301700204.

[8] El-Hage Y, Hind S, Robitaille F. Thermal conductivity of textile reinforcements for composites. J Text Fibrous Mater 2018;1:1–12. https://doi.org/https://doi.org/10.1177/2515221117751154.

[9] Twardowski TE, Lin SE, Geil PH. Curing in Thick Composite Laminates: Experiment and Simulation. J Compos Mater 1993;27:216–50. https://doi.org/https://doi.org/10.1177/002199839302700301.

[10] Bogetti TA, Gillespie JW. Process-Induced Stress and Deformation in Thick-Section Thermoset Composite Laminates. J Compos Mater 1992;26:626–60.

https://doi.org/https://doi.org/10.1177/002199839202600502.

[11] Wieland B, Ropte S. Process Modeling of Composite Materials for Wind-Turbine Rotor Blades: Experiments and Numerical Modeling. Materials (Basel) 2017;10:1157–69. https://doi.org/https://doi.org/10.3390/ma10101157.

[12] Maguire JM, Nayak K, Ó Brádaigh CM. Characterisation of epoxy powders for processing thick-section composite structures. Mater Des 2018;139:112–21. https://doi.org/10.1016/J.MATDES.2017.10.068.

[13] Mamalis D, Flanagan T, Ó Brádaigh CM. Effect of fibre straightness and sizing in carbon fibre reinforced powder epoxy composites. Compos Part A Appl Sci Manuf 2018;110:93–105. https://doi.org/https://doi.org/10.1016/j.compositesa.2018.04.013.

[14] Mamalis D, Murray JJ, McClements J, Tsikritsis D, Koutsos V, McCarthy ED, et al. Novel carbon-fibre powder-epoxy composites: Interface phenomena and interlaminar fracture behaviour. Compos Part B Eng 2019:107012. https://doi.org/10.1016/J.COMPOSITESB.2019.107012.

[15] Allred RE, Wesson SP, Babow DA. Powder Impregnation Studies for High Temperature Towpregs. SAMPE J 2004;40:40–8.

[16] Maguire JM, Simacek P, Advani SG, Ó Brádaigh CM. Novel epoxy powder for manufacturing thick-section composite parts under vacuum-bag-only conditions. Part I: Through-thickness process modelling. Compos Part A Appl Sci Manuf 2020;In review.

[17] Centea T, Hubert P. Measuring the impregnation of an out-of-autoclave prepreg by micro-CT. Compos Sci Technol 2011;71:593–9. https://doi.org/10.1016/j.compscitech.2010.12.009.

[18] Centea T, Hubert P. Modelling the effect of material properties and process parameters on tow impregnation in out-of-autoclave prepregs. Compos Part A Appl Sci Manuf 2012;43:1505–13. https://doi.org/https://doi.org/10.1016/j.compositesa.2012.03.028.

[19] Cender TA, Simacek P, Advani SG. Resin film impregnation in fabric prepregs with dual length scale permeability. Compos Part A Appl Sci Manuf 2013;53:118–28. https://doi.org/https://doi.org/10.1016/j.compositesa.2013.05.013.

[20] Centea T, Hubert P. Out-of-autoclave prepreg consolidation under deficient pressure conditions. J Compos Mater 2013;48:2033–45.

https://doi.org/https://doi.org/10.1177/0021998313494101.

[21] Helmus R, Centea T, Hubert P, Hinterhölzl R. Out-of-autoclave prepreg consolidation: Coupled air evacuation and prepreg impregnation modeling. J Compos Mater 2016;50:1403–13. https://doi.org/https://doi.org/10.1177/0021998315592005.

[22] Gutowski TG, Cai Z, Bauer S, Boucher D, Kingery J, Wineman S. Consolidation Experiments for Laminate Composites. J Compos Mater 1987;21:650–69. https://doi.org/https://doi.org/10.1177/002199838702100705.

[23] Shin DD, Hahn HT. Compaction of Thick Composites: Simulation and Experiment. Polym Compos 2004;25:49–59. https://doi.org/https://doi.org/10.1002/pc.20004.

[24] Bogetti TA, Gillespie JW. Two-Dimensional Cure Simulation of Thick Thermosetting Composites. J Compos Mater 1991;25:239–73. https://doi.org/https://doi.org/10.1177/002199839102500302.

[25] Sorrentino L, Polini W, Bellini C. To design the cure process of thick composite parts: experimental and numerical results. Adv Compos Mater 2014;23:225–38. https://doi.org/https://doi.org/10.1080/09243046.2013.847780.

[26] Maguire JM, Doyle A, Ó Brádaigh CM. Process modelling of thick-section tidal turbine blades using low-cost fibre reinforced polymers. 12th Eur. Wave Tidal Energy Conf., Cork, Ireland: 2017.

[27] Maguire JM, Nayak K, Glennon C, Robert C, Ó Brádaigh CM. Experimental validation of process simulations for vacuum-bag-only prepregs in thick-section structures. 14th Int. Conf. Flow Process. Compos. Mater., Luleä, Sweden: 2018.

[28] Johns Manville. Single-end Roving Selector Guide. 2018.

[29] ÉireComposites Teo. GRN 918 Datasheet. 2013.

[30] Goodfellow. Duratec 750 Datasheet. 2019.

[31] Kim D, Centea T, Nutt SR. Out-time effects on cure kinetics and viscosity for an out-of-autoclave (OOA) prepreg: Modelling and monitoring. Compos Sci Technol 2014;100:63–9. https://doi.org/https://doi.org/10.1016/j.compscitech.2014.05.027.

[32] Grunenfelder LK, Centea T, Hubert P, Nutt SR. Effect of room-temperature out-time on tow impregnation in an out-of-autoclave prepreg. Compos Part A Appl Sci Manuf 2013;45:119–26.

https://doi.org/https://doi.org/10.1016/J.COMPOSITESA.2012.10.001.

[33] Xue S, Barlow JW. Thermal Properties of Powders. Proc. 1990 Int. Solid Free. Fabr. Symp., 1990, p. 179–85.

[34] Tian X, Peng G, Yan M, He S, Yao R. Process prediction of selective laser sintering based on heat transfer analysis for polyamide composite powders. Int J Heat Mass Transf 2018;120:379–86. https://doi.org/https://doi.org/10.1016/J.IJHEATMASSTRANSFER.2017.12.045.

[35] Greco A, Maffezzoli A. Polymer Melting and Polymer Powder Sintering by Thermal Analysis. J Therm Anal Calorim 2003;72:1167–74. https://doi.org/https://doi.org/10.1023/A:1025096432699.

[36] Celle P, Drapier S, Bergheau J-M. Numerical modelling of liquid infusion into fibrous media undergoing compaction. Eur J Mech - A/Solids 2008;27:647–61. https://doi.org/10.1016/j.euromechsol.2007.11.002.

[37] Grunenfelder LK, Nutt SR. Void formation in composite prepregs – Effect of dissolved moisture. Compos Sci Technol 2010;70:2304–9. https://doi.org/https://doi.org/10.1016/j.compscitech.2010.09.009.

[38] Maguire JM. Processing of Thick Section Epoxy Powder Composite Structures. PhD Thesis, The University of Edinburgh, 2019.

[39] Padaki S, Drzal LT. A simulation study on the effects of particle size on the consolidation of polymer powder impregnated tapes. Compos Part A Appl Sci Manuf 1999;30:325–37. https://doi.org/https://doi.org/10.1016/S1359-835X(98)00115-8.

[40] O&M Heater Co. Ltd. Products - Silicone Rubber Heater - Stretch Type 2018. http://om-heater.jp/english/products/srh_strc.html (accessed December 6, 2018).

[41] Saldívar-Guerra E, Vivaldo-Lima E. Handbook of polymer synthesis, characterisation, and processing. 2013.

[42] Kravchenko OG, Kravchenko SG, Pipes RB. Chemical and thermal shrinkage in thermosetting prepreg. Compos Part A Appl Sci Manuf 2016;80. https://doi.org/https://doi.org/10.1016/j.compositesa.2015.10.001.

[43] Martinez GM. FAST CURES FOR THICK LAMINATED ORGANIC MATRIX COMPOSITES. Chem Eng Sci 1990;46:439–50.

https://doi.org/https://doi.org/10.1016/0009-2509(91)80005-J.

[44] Ruiz E, Trochu F. Multi-criteria thermal optimization in liquid composite molding to reduce processing stresses and cycle time. Compos Part A Appl Sci Manuf 2006;37:913–24. https://doi.org/https://doi.org/10.1016/j.compositesa.2005.06.010.

[45] Struzziero G, Skordos AA. Multi-objective optimisation of the cure of thick components. Compos Part A Appl Sci Manuf 2017;93:126–36. https://doi.org/https://doi.org/10.1016/J.COMPOSITESA.2016.11.014.

[46] Greenspec. Insulation materials and their thermal properties 2018.

Appendix A. Supplementary material

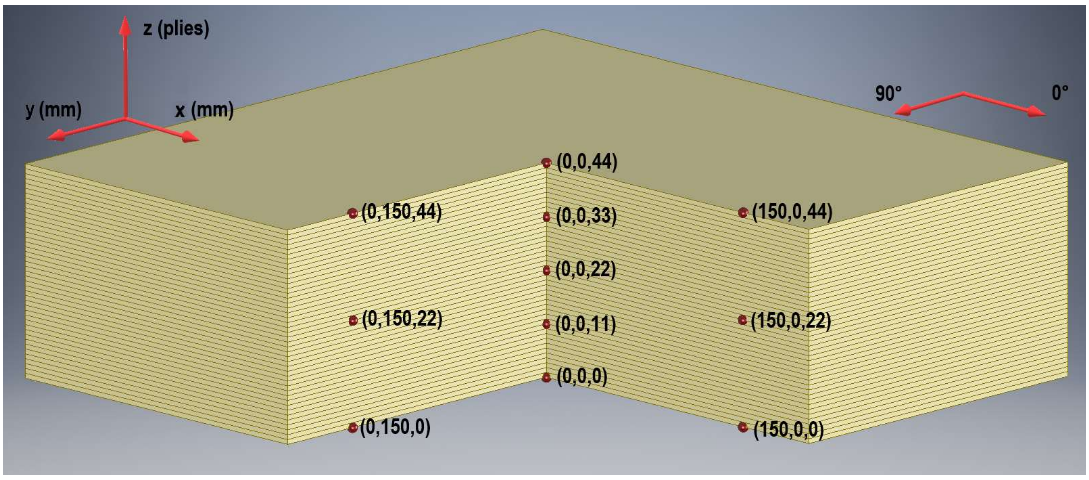

Figure A.1. Rendered image of Test Laminate 2 with a quarter section removed to reveal the position of the thermocouples. Refer to the axes (top left) for the coordinate system i.e. (x, y, z). The additional axes (top right) refer to the fibre direction.

Table A.1. Material properties used for the insulation and silicone rubber heating mat.

Property [units]	**Value**	**Source**
Thermal conductivity of insulation [W/m.K]	0.04	[46]
Thermal conductivity of silicone rubber [W/m.K]	0.53	[5]
Density of insulation [kg/m^3]	40.0	[46]
Density of aluminium [kg/m^3]	1540.0	[5]
Specific heat capacity of insulation [J/kg.K]	1030.0	[46]
Specific heat capacity of silicone rubber [J/kg.K]	1050.0	[5]

Checks for sources of experimental error

To check for thermal expansion effects, Test Laminate 1 was reheated after curing, shown in Figure A.2. Overall, it was found that the thermal expansion/contraction accounted for approximately ± 3% of the total thickness change of Test Laminate 1. This was considered negligible in terms of validating the process simulations. It should be noted, however, that the laminate appeared to initially contract upon heating, then subsequently expand. This feature was present for all three test laminates when reheated. It was noted that the response on cooldown was also non-linear, with a peak in expansion as the laminate underwent its glass transition. As such, the two phenomena may be linked, however, further investigation was outside the scope of this work.

As previously discussed, thermocouples were positioned at both the centre and near the edges of the laminate so that the 1D heat transfer assumption could be tested. It was found that a temperature difference did exist between the centre and edges (maximum of 13.5°C, but generally < 10°C), with the centre typically lagging behind the edges, as shown in Figure A.3. Nevertheless, the through-thickness temperature difference was large enough (maximum of 80°C) to dominate heat transfer within the laminate.

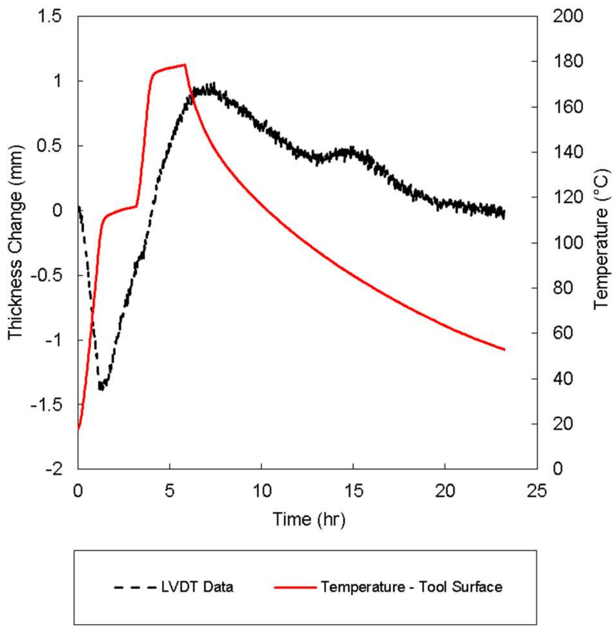

Figure A.2. Plot of LVDT data for a reheat cycle on Test Laminate 1. Overall, the change was negligible compared to the laminate thickness change during the initial processing.

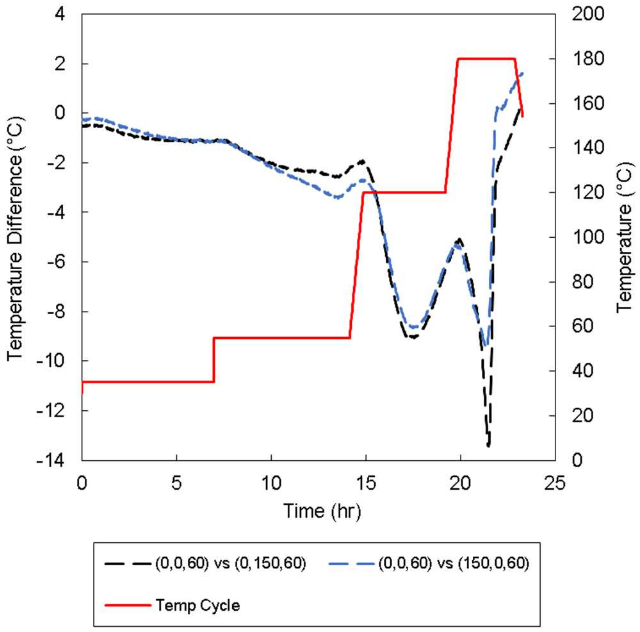

Figure A.3. Plot of the temperature difference between the centre of Ply 60 and 150 mm towards the edge, in the x and y directions (for Test Laminate 1). In both cases, the centre thermally lags the edges, hence the negative values. The legend refers to the coordinate system given in Figure A.1.

Results of Test Laminate 3

Efforts were made to reduce the in-plane temperature difference for the other test laminates by fitting the insulation tighter to their sides to prevent heat loss via gaps between the laminate and the insulation. In this regard, the in-plane dimensions of Test Laminate 3 were increased to 420 mm x 420 mm.

The target FVF for Test Laminate 3 was also changed to 0.45 to reduce any potential pressure sharing effects i.e. it has been suggested for VBO prepregs that, as the resin layers diminishes, the fibre-bed may begin to share some of the pressure applied by the vacuum bagging [19]. The low temperature drying stage (at 35°C) was also replaced with a continuous drying stage at 55°C to ensure the sintering process finished before the impregnation stage began.

The results for Test Laminate 3 are shown in Figure A.4. The simulations showed reasonable accuracy in capturing the general trends of the experiments, however, they were slightly inaccurate in predicting the thickness change due to sintering, which has a knock-on effect with the accuracy of the temperature profile during the drying stage. It was found that, when the whole drying stage was carried out at 55°C, sintering ceased after approximately 10 hr and the thickness change became dependent on inter-tow resin flow, which was slow at this temperature due to the high viscosity of the resin. Once again, the resin flow model predicted a noticeable transition from inter-tow flow to intra-tow flow during the impregnation stage and an abrupt end to thickness change, whereas, the LVDT data suggested a more gradual transition between inter-tow flow and intra-tow flow, and a more gradual cessation to thickness change. A section was cut from Test Laminate 3, and, upon inspection, it was confirmed that the laminate suffered from the same defects as Test Laminate 1 i.e. incomplete tow impregnation and inter-tow voids. Furthermore, Test Laminate 3 showed ± 7% thickness variation along the cut edge and an in-plane temperature variation similar to Test Laminate 1.

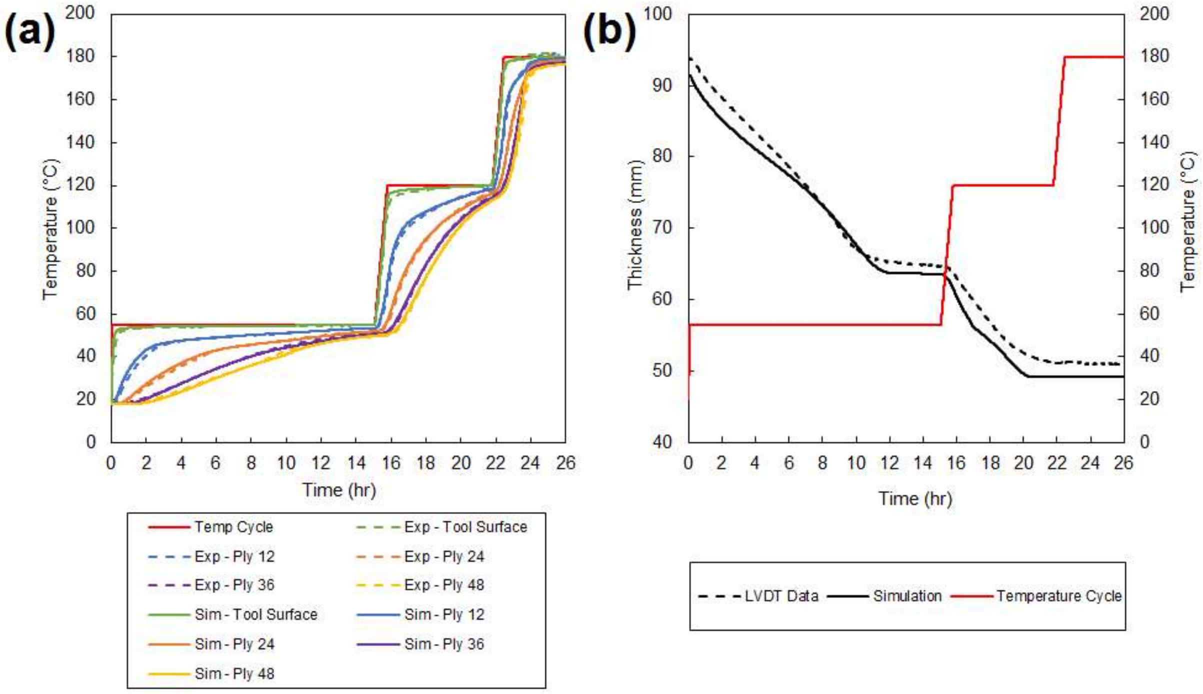

Figure A.4. Comparison of experimental data and simulated results for Test Laminate 3: (a) thermocouple data compared with simulated tempatures; (b) LVDT data compared with simulated thickness change.

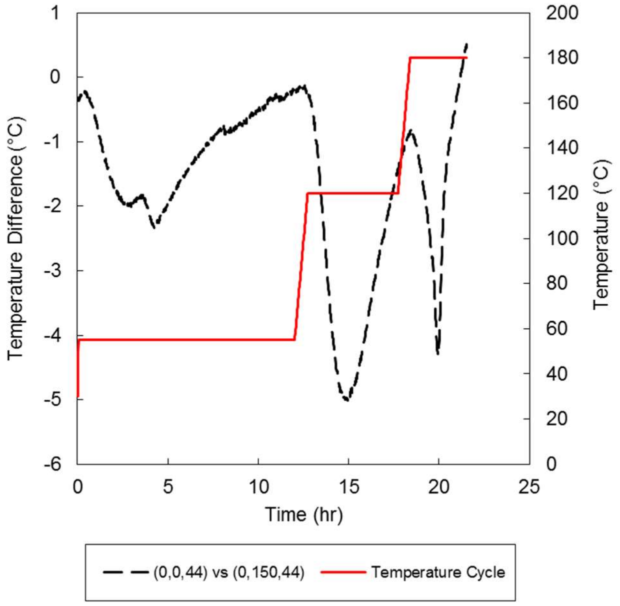

Figure A.5. Plot of the in-plane temperature difference between (0,0,44) and (0,150,44) in Test Laminate 2. Refer to Figure A.1 for the coordinate system.

Table A.2. Initial conditions used for the 100-ply process simulations.

Parameter [units]	Value
No. of plies	100
Cured ply thickness [mm]	1.0
Fibre volume fraction	0.5
Degree of impregnation	0.113
Powder void fraction	0.485
Degree of cure	0.01
Applied pressure [Pa]	90×10^3
Laminate/bagging/tool temperature [°C]	23

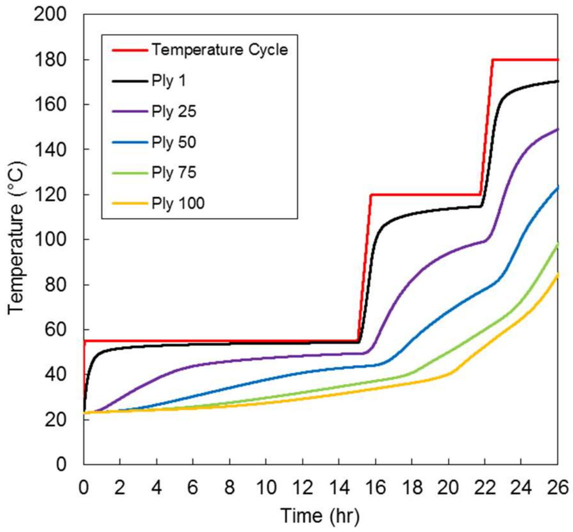

Figure A.6. Simulated temperatures in a 100-ply laminate manufactured using a heated steel tool, and 200 mm insulation at the top boundary. The laminate consisted of UD GF and epoxy powder (GRN 918).

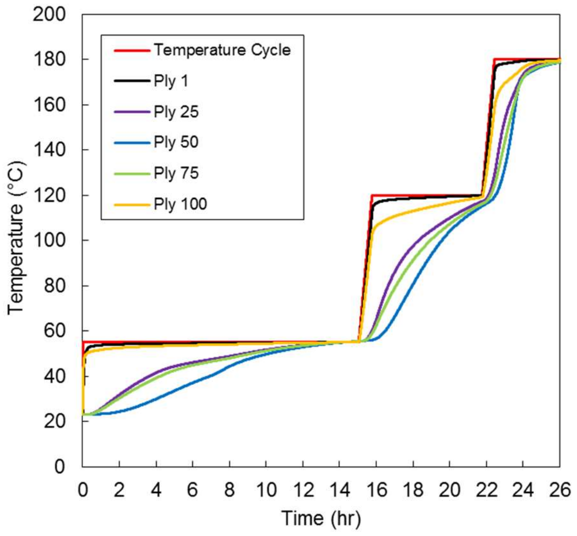

Figure A.7. Simulated temperatures in a 100-ply laminate manufactured using a heated steel tool (underneath Ply 1), and a silicone rubber heating mat at the top boundary. The laminate consisted of UD GF and epoxy powder (GRN 918).

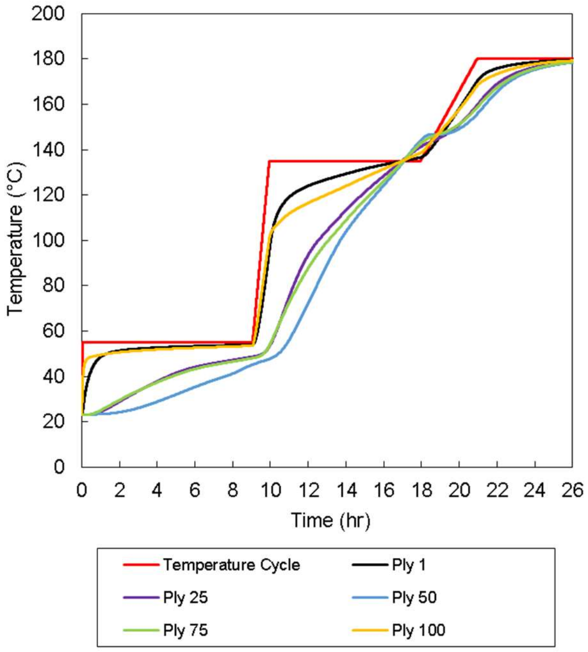

Figure A.8. Simulated temperatures for a 100-ply thick laminate processed using a modified cycle. Note that there was a small overshoot in temperature at the end of the impregnation stage. This was due to the higher dwell temperature used for the modified cycle (i.e. 135°C for the impregnation stage). The higher temperature increased the rate of curing, which resulted in a relatively small build-up of heat.

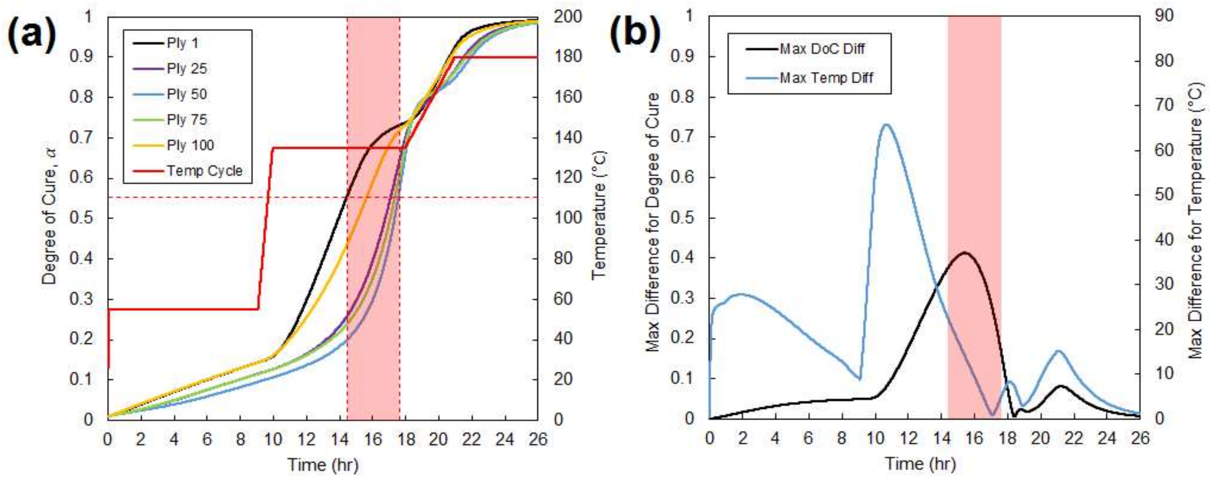

Figure A.9. (a) Simulated DoC evolution for the modified temperature cycle. The horizontal dashed red line represents the gel point ($\alpha_g = 0.56$ [12]), and the shaded red area highlights the duration of gelation in the laminate. (b) Maximum temperature difference and maximum DoC difference for the modified temperature cycle. The temperature difference was significantly reduced during gelation, while the peak in DoC difference was reduced by approximately 0.1.